Chemical Science

ROYAL SOCIETY OF CHEMISTRY

EDGE ARTICLE

View Article Online
View Journal | View Issue

Cite this: *Chem. Sci.*, 2021, **12**, 9442

All publication charges for this article have been paid for by the Royal Society of Chemistry

Accessing lanthanide-based, *in situ* illuminated optical turn-on probes by modulation of the antenna triplet state energy†

Alexia G. Cosby, [a] Joshua J. Woods, [b] Patrick Nawrocki, [c] Thomas J. Sørensen, [c] Justin J. Wilson [b] and Eszter Boros *[a]

Received 16th April 2021
Accepted 13th June 2021

DOI: 10.1039/d1sc02148f

rsc.li/chemical-science

Luminescent lanthanides possess ideal properties for biological imaging, including long luminescent lifetimes and emission within the optical window. Here, we report a novel approach to responsive luminescent Tb(III) probes that involves direct modulation of the antenna excited triplet state energy. If the triplet energy lies too close to the $^5D_4$ Tb(III) excited state (20 500 cm^{-1}), energy transfer to $^5D_4$ competes with back energy transfer processes and limits lanthanide-based emission. To validate this approach, a series of pyridyl-functionalized, macrocyclic lanthanide complexes were designed, and the corresponding lowest energy triplet states were calculated using density functional theory (DFT). Subsequently, three novel constructs **L3** (nitro-pyridyl), **L4** (amino-pyridyl) and **L5** (fluoro-pyridyl) were synthesized. Photophysical characterization of the corresponding Gd(III) complexes revealed antenna triplet energies between 25 800 and 30 400 cm^{-1} and a 500-fold increase in quantum yield upon conversion of Tb(**L3**) to Tb(**L4**) using the biologically relevant analyte H_2S. The corresponding turn-on reaction can be monitored using conventional, small-animal optical imaging equipment in presence of a Cherenkov radiation emitting isotope as an *in situ* excitation source, demonstrating that antenna triplet state energy modulation represents a viable approach to biocompatible, Tb-based optical turn-on probes.

Introduction

The optical probe mediated detection of changes in receptor, enzyme or analyte expression can reveal disease-related biological activity such as aberrant enzymatic activity,[1–4] modification of intracellular pH,[5–7] production of reactive oxygen species,[8] or drastic changes in the extra- and intracellular concentration of analytes such as metal cations,[9–12] or inorganic salts.[13] Ideally, such optical responsive probes produce a ratiometric response, but *in lieu* of this, a measurable turn-on effect is preferred over turn-off response, as the absence of an optical signal can be quenched by factors other than the lack of analyte. Organic chromophores have been extensively explored and established as tools for probing intra- and extracellular biochemistry. The luminescence emission from discrete lanthanide complexes provides an attractive alternative to organic chromophores for biological imaging applications.[14] Lanthanide luminescence produces narrow emission bands within the optical window with diminished photobleaching, large pseudo-Stokes shifts, and long luminescent lifetimes that enable time-resolved imaging applications. However, the need of short-wave UV excitation of sensitizing antennae outside the biological optical window, especially for Tb(III), has limited the use of lanthanide-based sensing probes to *in cellulo* experiments. In our previous work, we have successfully demonstrated that Cherenkov radiation (CR) of positron-emissive radioisotopes can serve as an *in situ* excitation source and thus opens opportunities for lanthanide-based *in vivo* optical imaging.[15,16] Motivated by these results, we hypothesized that the *in situ* excitation of Tb(III)-based turn-on probes in presence of a CR emissive isotope could provide means to detect the aberrant levels of biologically relevant analytes *in vivo*. Based on our prior work, we had determined, that CR-mediated excitation of Tb(III)-complexes low μM concentrations required Tb-based quantum yields (Φ_{Tb}) of at least 0.1 or above. We therefore proposed that a toggle between Φ_{Tb} <0.01 ("off") and Φ_{Tb} >0.05 ("on") could produce a detectable Tb(III) turn-on signal in the presence of a CR emissive isotope.

Several strategies have previously been pursued to devise responsive, luminescent lanthanide complexes. The efficient excitation of lanthanide excited states relies on energy transfer from an organic chromophore within the immediate coordination environment of the lanthanide ions.[17–20] Hence, the modification of the

[a]*Department of Chemistry, Stony Brook University, Stony Brook, New York, 11794, USA. E-mail: eszter.boros@stonybrook.edu*

[b]*Department of Chemistry and Chemical Biology, Cornell University, Ithaca, New York, 14853, USA*

[c]*Nano-Science Center & Department of Chemistry, University of Copenhagen, Universitetsparken 5, 2100, København Ø, Denmark*

† Electronic supplementary information (ESI) available. See DOI: 10.1039/d1sc02148f

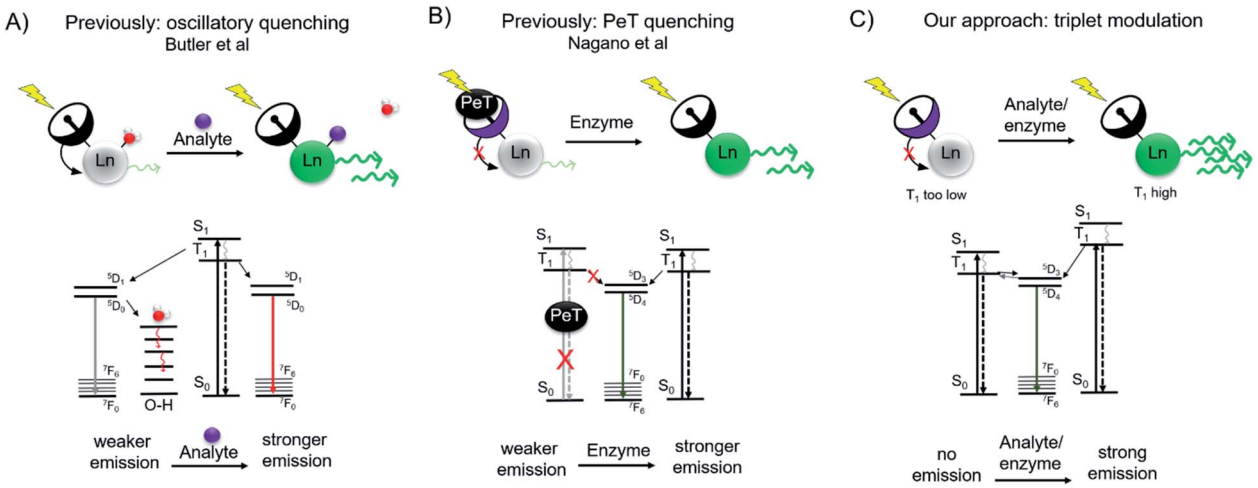

Fig. 1 Schematic and accompanying Jablonksi diagrams of previous approaches (A and B) and our approach (C) to lanthanide-based turn-on probes for analyte or enzyme sensing. (A) Lanthanide emission is quenched through O–H oscillators until an analyte replaces the coordination water molecule.[21] (B) Antenna chromophore possesses a photoelectron (PeT) quencher, limiting excitation into the excited singlet state (S_1) and subsequent energy cascade to lanthanide excited state. Enzymatic cleavage releases the PeT quencher.[26] (C) Our approach is the direct modulation of the antenna triplet excited state (T_1), where interaction with analyte or enzyme would increase T_1 to enable efficient energy transfer to the lanthanide excited state.

efficiency of this energy transfer process provides a convenient handle for turn-on probes. One approach includes the reduction of oscillatory quenching upon coordination of an analyte of interest to the first coordination sphere, effectively replacing a water molecule (Fig. 1A). This has been explored for the sensing of F^-, where corresponding Eu(III) emission increases 9-fold upon binding of F^-, demonstrating fluoride sensing at concentrations of as low as 20 μM.[21] Inner-sphere water displacement has also been employed to detect CN^-, HCO_3^-, and ATP.[22–24] A second approach explores the caging of the organic antenna chromophore upon enzyme activity. Borbas and coworkers have demonstrated the feasibility of this approach by enzyme triggered assembly of the lanthanide-sensitizing antenna (coumarin). The formation of the coumarin antenna sensitizes Tb(III) or Eu(III) 5- to 10-fold more efficiently as compared to the benzoyl-precursor, with "turn-on" probe quantum yields of 0.010 and 0.016 for Eu(III) and Tb(III) respectively.[25] A third approach involves the photoelectron transfer (PeT) mediated quenching of antenna emission (Fig. 1B). A Tb(III)-probe developed by Nagano and coworkers employed a photoelectron transfer quencher directly coordinated to the aniline antenna moiety, resulting in intraligand quenching of the antenna excited triplet state (T_1).[26] Upon reaction with *N*-acetyltransferase, the PeT quenched antenna was converted into an optically active probe producing a 10-fold increase in emission as determined by time-resolved microscopy.

In addition to the presence of oscillatory quenchers, caged antennae or PeT quenchers, the relative quantum yield of lanthanide complexes relies on the efficient energy transfer from the dye to the electronic energy levels of the lanthanide ion, which requires rates of energy transfer from the excited states of the antenna to the lanthanide center that can compete with the rates of the other active pathways of deactivation in the antenna.[27] The importance of the relative energies of T_1 and the $^5D_{0/1}$ levels for Eu(III), and the $^5D_4$ for Tb(III) has been discussed and demonstrated extensively by Latva, Raymond, Parker and others.[27–30]

While many literature examples have demonstrated elimination of a luminescence quencher as described above, no attempts have yet been made to modify the antenna triplet state directly and irreversibly. Parker and coworkers observed an increase in the excited triplet state energy (21 300 cm^{-1} to 22 000 cm^{-1}) upon protonation of phenathridine-antenna Eu(III)/Tb(III) complexes (see ESI Fig. S2†).[7] The Φ_{Tb} increased 27-fold to 0.025 at pH 6.5–7, although the Φ_{Eu} only increased (3-fold) upon protonation at pH 1.5, which is outside of the physiological pH range.

A significant drawback of each one of these approaches (Fig. 1 & S1†) is the low quantum yield (Φ_{Ln}) of the corresponding turn-on probes resulting in limited brightness, rendering them not applicable for bioimaging applications beyond time-resolved microscopy (for a summary of primary turn-on examples see Table S1†). Furthermore, the low Φ_{Ln} of these compounds, even in the on-state, would not produce signal in presence of a CR emitter.

Here, we propose that the triplet energy level can be adjusted by direct and irreversible functional group transformation of the antenna, providing unprecedented access to activatable lanthanide probes with comparatively high quantum yields in their corresponding turn-on state. As we demonstrate, these activatable lanthanide probes are ideal candidates for biological optical imaging with Cherenkov-radiation, owing to the high energy wavelengths (~200–400 nm) required for excitation.

Here, we designed a library of lanthanide complexes baring antennae with varying T_1 energies relative to the lanthanide excited state, allowing for subsequent and irreversible chemical modification of the antenna in a single step (*i.e.* reduction) to produce antennae capable of efficiently sensitizing Tb(III). Guided by density functional theory calculations of the ground

state energy of antenna singlet and triplet states, we selected Tb(**L3**) ("off"), Tb(**L4**) and Tb(**L5**) (both "on"). Following chemical synthesis and characterization, the photophysical properties of each complex were measured, including relative T_1 energy levels, quantum yields and turn-on response to a biologically relevant analyte (H_2S) in presence of a CR emitter as an *in situ* excitation source.

Results and discussion

Molecular design and DFT

We designed and synthesized a series of terbium(III) complexes which utilize a macrocyclic chelator based on cyclen, and a pyridyl antenna which incorporates varied substituents at the para-position (Fig. 2). The chelator forms kinetically inert and highly stable Ln(III) complexes, with the coordinating pyridyl substituent forming an 8-coordinate complex.[31] We proposed that tuning of the triplet state energy can be achieved by single-step chemical modification of the antenna substituent.

According to Latva's empirical principle, the lowest energy antenna triplet excited state should be at least 1800 cm^{-1} above the photoluminescent lanthanide excited state.[27] If the change in energy between these states is too low, back energy transfer processes become more probable, leading to severely diminished lanthanide-based radiative de-excitation and increased ligand-based phosphorescence/fluorescence. Modulation of triplet energy of pyridyl and picolinate-based antennas can be induced by the incorporation of electron-withdrawing substituents such as nitro, cyano or carbonyl groups which are expected to lower the relative ligand triplet energy. This has been observed previously by Faulkner and Sherry, who reported a nitro-substituted antennae with decreased lanthanide luminescence.[32,33] In contrast, electron-donating functional groups such as amines, effectively increase the ligand triplet state energy.[29]

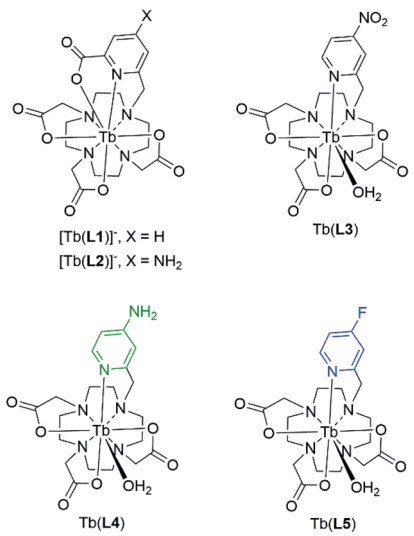

Fig. 2 Structures of previously investigated complexes $[Tb(\mathbf{L1})]^-$ and $[Tb(\mathbf{L2})]^-$, leading to the design and of Tb(**L3**)–Tb(**L5**) featured in this study.

In our previous study, we observed a 1.4-fold increase in Φ_{Tb} with a picolinate antenna incorporating an amine in the para position $[Tb(\mathbf{L2})]^-$, when compared to the corresponding picolinate antenna $[Tb(\mathbf{L1})]^-$ (Fig. 2).[16] We attributed this increase to the 1330 cm^{-1} blue-shift of the triplet excited state energy for $[Tb(\mathbf{L2})]^-$ relative to $[Tb(\mathbf{L1})]^-$, which decreases the likelihood of a back energy transfer to the antenna. The high quantum yield of $[Tb(\mathbf{L2})]^-$ motivated the design of an antenna that possessed a poor triplet energy match and could be transformed into the *para*-NH_2-picolinate for a particularly efficient luminescence turn-on. Inspired by work from others on nitro-to-amine reduction mediated sensing with organic fluorophores, we proposed a nitro-moiety could operate as the "off" state.[34–38] Synthetic challenges to furnish the nitro-picolinate precursor (ethyl 6-(bromomethyl)-4-nitro-2-pyridinecarboxylate) derivative of $[Tb(\mathbf{L2})]^-$ in sufficient quantities led to the design of Tb(**L3**), a more readily accessible coordination complex. In addition to the electron-donating amine of Tb(**L4**), we hypothesized that a fluoro-substituted complex Tb(**L5**) could also provide a sufficiently blue-shifted T_1 relative to the nitro-moiety.

To predict the relative T_1 energies of the Tb(III) complexes in the presence of the antenna bearing different substituents, we carried out density functional calculations (DFT) at the TPSSh/LCRECP/6-31G(d,p) level of theory. The complexes were optimized in the ground state singlet state (GS) in gas phase and the T_1 energies were estimated using the adiabatic-transition approach, where the energy difference between T_1 and GS corresponds to the optimized geometry of each state. This method gives the lowest energy difference between the S_0 and T_1 states, corresponding to the 0–0 emission energy. In contrast, the commonly used vertical approach, where T_1 and the S_0 share the same geometry, gives a larger energy gap, since the calculated T_1 state exists in a vibrationally excited state.[39–41] Solvation effects were included in the calculations using the solvent model based on density (SMD) method and the previously optimized polarizable continuum model (PCM) radius was used for Tb(III) in all solvation calculations without scaling ($\alpha = 1.0$).[42] Spin density plots of the optimized T_1 state for all of the complexes confirmed that the spin density was located on the antenna arm of the ligand (Fig. 3A). In agreement with our hypothesis, the calculated T_1 energy of Tb(**L3**) is significantly lower than that of Tb(**L4**) and Tb(**L5**) (Table 1).

Synthesis

After affirming our original hypothesis with DFT, we embarked on the chemical synthesis of the **L3**, **L4** and **L5** ligand systems. **L3** was synthesized by alkylating tri-*tert*-butyl protected macrocycle (^{t}Bu-DO3A, tri-*tert*-butyl 1,4,7,10-tetraazacyclododecane-1,4,7-triacetate) with a *para*-nitropyridyl chromophore [2-methyl(sulfonyloxymethyl)-4-nitropyridine], which was synthesized in three steps from commercially available 2-methylpyridine *N*-oxide to yield *tert*-butyl protected intermediate **S1** (for a synthesis scheme, see ESI Fig. S1†). Subsequent deprotection under acidic conditions produced **L3**. To afford the electron-donating amine substituent, compound **S1** was reduced by Pd-catalyzed hydrogenation and purified using semi-

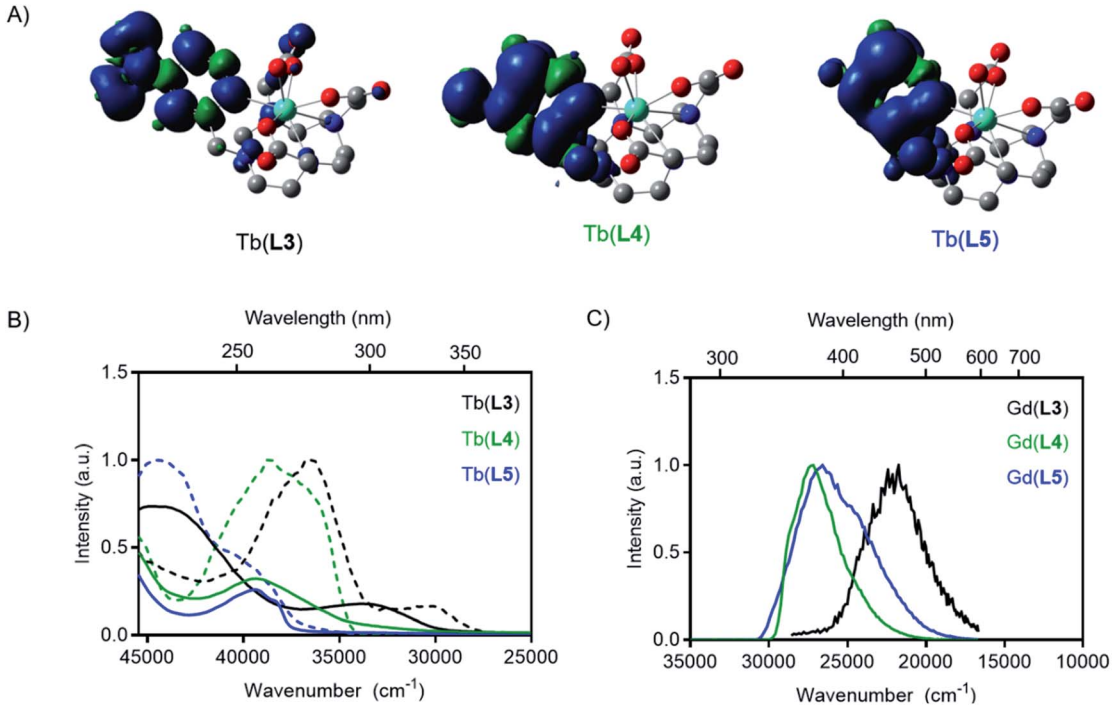

Fig. 3 (A) Spin-density plots of optimized T_1 state of each Tb(III) complex. (B) Absorbance (solid) and excitation (dashed) spectra of Tb(III) complexes. (C) Phosphorescence spectra of Gd(III) complexes. All measurements in PBS buffer at RT (absorption, excitation) or 77 K (phosphorescence).

Table 1 Summary of photophysical properties of Tb(III) complexes studied in this work[a]

Compound	Experimental[b] S_1 (cm^{-1})	Experimental[b] T_1 (cm^{-1})	Calculated T_1 (cm^{-1})	Φ_{Tb}[c]	q[d]	x-fold Φ_{Tb} increase[e]
Tb(**L3**)	33 333	25 773	17 307	0.0002	1.3	—
Tb(**L4**)	38 462	29 586	26 625	0.10	1.1	500
Tb(**L5**)	39 370	30 395	27 063	0.093	0.9	465

[a] All experimental values recorded in PBS buffer. [b] Measured on Gd(III) complex. [c] Estimated relative error 10–15%. [d] Hydration state (±20%) values calculated according to literature methods. [e] Relative to Tb(**L3**).

preparative HPLC to yield **S2**, followed by deprotection under acidic conditions to provide ligand **L4**. The fluorinated substituent **L5** was synthesized by alkylation of 2-(bromomethyl)-4-fluoropyridine (synthesized in one step from 4-fluoro-2-methylpyridine) with ^{t}Bu-DO3A, followed by deprotection of precursor **S3** under acidic conditions. Tb(III) complexes were formed in water by mixing the Tb(III) with ligand under acidic conditions followed by adjustment of pH to 7 and removal free Tb(III) by reverse phase chromatography.

Photophysical measurements

Photophysical measurements of each Tb(III) complex were carried out to determine how substituents on the ligand pyridine influenced T_1 and overall quantum yield. For each complex, the spectrochemical properties were measured in PBS (pH = 7.0) at room temperature, including absorption, emission spectra, and corresponding quantum yields. Luminescent lifetime values of all complexes were determined in PBS and D_2O to determine inner-sphere hydration (q).[43] A summary of the results is provided in Table 1. A 5200 cm^{-1} blue-shift was observed in the experimental absorbance maxima from Tb(**L3**) to Tb(**L4**), indicating an increase in the relative excited singlet state energies (Fig. 3). Similarly, a blue-shift of the absorbance maximum was observed for the modification of Tb(**L3**) to complex Tb(**L5**) (6000 cm^{-1}).

Time-gated phosphorescence spectra were recorded at 77 K for Tb(III) and Gd(III) complexes of **L3**, **L4** and **L5** ligands. The energy of the excited T_1 states were determined as the onset of the phosphorescence emission peak from the Gd(III) complexes (see ESI†). As the lanthanide-based excited state of Gd(III) is too high in energy (32 200 cm^{-1}) to be excited by the ligands studied, the result is pure ligand-based emission. The absorbance and excitation spectra of Tb(III) complexes, as well as the phosphorescence emission from the T_1 state obtained from the Gd(III) complexes are shown in Fig. 3.

The phosphorescence excitation spectra of the Gd(III) complexes are in good agreement with the steady-state absorption measurements. Excitation measurements of the Tb(III) complexes however revealed that two absorbing species are simultaneously present in all samples (See Fig. 3 and in ESI, Fig. S9 to S12†). The excitation spectrum obtained when monitoring Tb(III)-based emission result in a blue shifted excitation spectrum compared to the excitation spectrum obtained when monitoring ligand-based emission. The two excitation spectra appear to agree with the neutral and the protonated forms of the pyridyl groups that exist in an equilibrium at the PBS moderated pH under the cryogenic, 77 K measurement conditions. At room temperature, the protonated species is not readily detected, leading to the conclusion that it does not play a significant role in the modulation of emission properties or the de-excitation pathway of M(**L4**) complexes in subsequent experiments.

The absorption and excitation spectra of **L3** have many components, but a low intensity peak at 330 nm resembling the charge transfer band was observed, and the T_1 state was readily accessed by excitation through the charge transfer band. Like the absorption maxima, the triplet excited states also resulted in a blue shift of Gd(**L4**) and Gd(**L5**) relative to Gd(**L3**). The experimental triplet state energy of **L3** was only 5700 cm^{-1} greater than the $^5D_4$ level for Tb(III), while the experimental triplet energy of **L4** and **L5** are 9500 and 9900 cm^{-1} greater respectively. The variation in T_1 indicates competing back energy transfer pathways for **L3** reduce overall Tb(III) sensitization. A further explanation for decreased Tb(III) emission of **L3** could be that the energy cascade from the lowest-lying excited T_1 state populates the $^5D_3$ state and is subsequently quenched by oxygen before populating the $^5D_4$ excited state.[44] The DFT-calculated and experimentally determined T_1 values follow the same trend, where reduction or conversion of **L3** to **L4** or **L5** increases the triplet state energy level.

Quantum yield measurements were carried out as described previously, using $[Tb(\mathbf{L1})]^-$ (Φ_{Ln} = 0.47) as the reference compound.[16] Quantum yield was 0.0002 for Tb(**L3**), which corresponds well to diminished efficiency of transfer from the corresponding T_1 state. Substitution of the electron-withdrawing nitro-substituent (**L3**) with an amine (**L4**), increased the quantum yield of Tb(**L4**) 500-fold, to 0.10. Similarly, replacement of the nitro-group with a fluoro-group improves the quantum yield 465-fold to 0.09 for Tb(**L5**), also in agreement with a significant blue shift of T_1. Albeit trends predicted by our DFT calculations persist, we note a deviation of 3000–8000 cm^{-1}. This indicates that instead of the existence of a T_1 energy level energy transfer threshold that correlates with the $^5D_4$ excited state, rather the rate of back energy transfer appears to control the efficiency of the lanthanide based de-excitation.

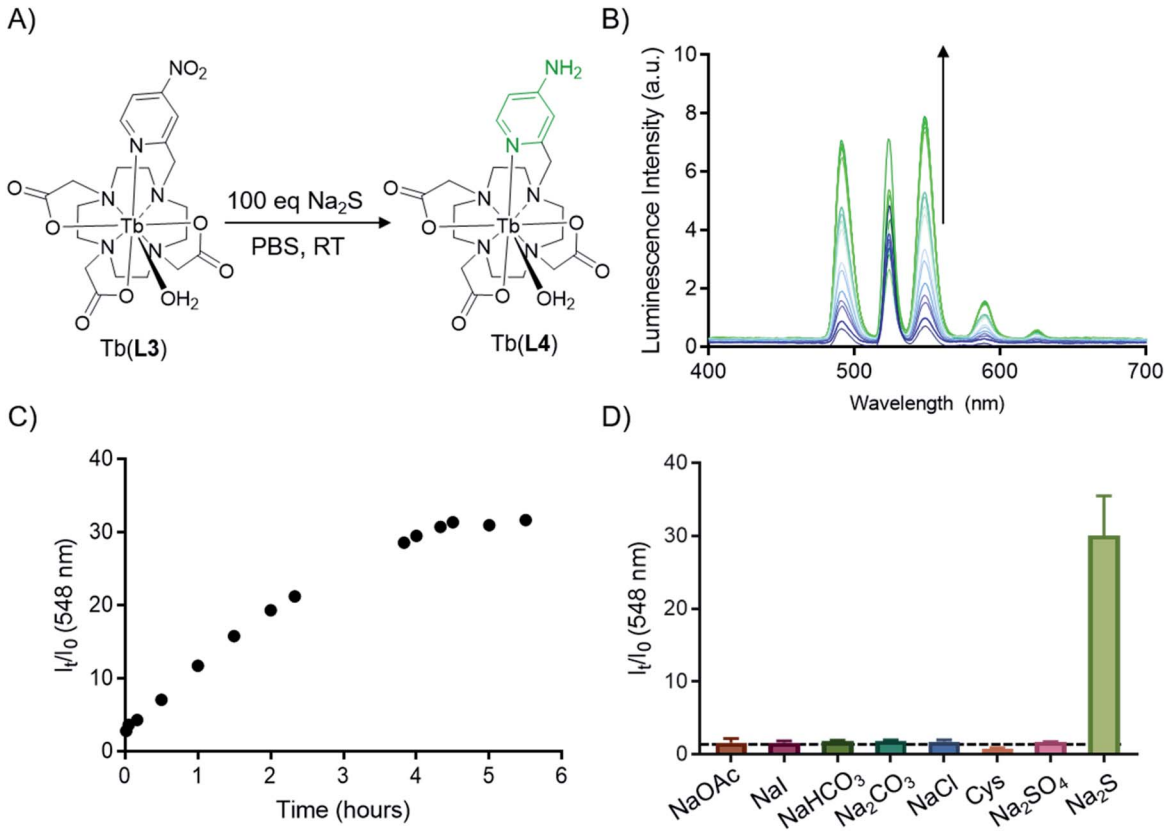

Fig. 4 (A) Reaction scheme of Tb(**L3**) (10 μM) reacting with 100 equiv. Na_2S (1 mM) to form Tb(**L4**) *in situ*. (B) Emission spectra over time upon reduction of 10 nmol (10 μM) Tb(**L3**) (523 nm peak = scattering). (C) Fold-increase of emission over 5.5 hours. (D) Relative fold-change of emission of 10 nmol (10 μM) Tb(**L3**) in response to NaOAc, NaI, $NaHCO_3$, NaCl, Na_2SO_4, Cys, and Na_2S (100 equiv.) in PBS (dashed line = 1; error bars represent standard deviation, n = 3).

Hydrogen sulfide sensing

With evidence of the 500-fold quantum yield increase from Tb(III) complexes of **L3** and **L4**, reduction of Tb(**L3**) we sought to chemically transform Tb(**L3**) to Tb(**L4**) using a biologically relevant analyte. An analyte of biological importance, hydrogen sulfide has gained interest in the past decade in the context of non-invasive molecular imaging, as it plays important roles in apoptosis, insulin signaling, blood pressure regulation, and neuromodulation.[45,46] Previous H_2S sensitive optical probes rely on the presence of an accessible nitroaromatic component which acts as a PeT quencher, but in the presence of aqueous HS^- is reduced to an amine.[47,48] Motivated by the reactivity of previous nitroaromatic-containing metal complexes, we assessed Na_2S as an *in situ* H_2S source to reduce Tb(**L3**) without significant degradation of the corresponding complex (Fig. 4A). Indeed, in the presence of 100 equivalents of Na_2S, full conversion of Tb(**L3**) to Tb(**L4**) was obtained. The direct functional group transformation was followed by HPLC and further affirmed by mass spectrometry (ESI Fig. S21†). Of note, the reaction produced no detectable side products, which bodes well for selective sensing applications. The conversion reaction was also monitored *in situ* by measurement of increasing fluorescence emission produced by Tb(**L4**) in the presence of 100 equivalents of Na_2S (Fig. 4B). Plotting of relative intensity of the emission peak at 548 nm, corresponding to the diagnostic $^5D_4$–$^7F_5$ transition reveals a 31-fold increase over 5 hours, which is comparable to other H_2S-sensing systems.[48–50] Selectivity of Tb(**L3**) was tested against a series of biologically relevant anions and reducing agents such as NaOAc, NaI, $NaHCO_3$, Cys. A 31-fold increase was only obtained in the presence of Na_2S (Fig. 4D), while 100 equivalents of other analytes produced no detectable luminescence increase.

Optical imaging with CRET

To validate that our T_1 energy mediated probe turn-on produces an appropriate optical signal that can be readily detected using conventional, small animal imaging equipment, we conducted experiments in the presence of the Cherenkov emissive radioisotope ^{18}F ($\beta_{avg}^+ = 0.25$ MeV, 97%, $t_{1/2} = 109$ min). As we have previously shown, Cherenkov radiation (CR) provides a convenient *in situ* excitation source for luminescent Tb(III) complexes.[16] CR-imaging was carried out with complexes Tb(**L3**), Tb(**L4**), and Tb(**L5**), imaging phantoms containing 1–150 nmol probe (as measured by ICP-OES). Based on our previous CRET studies, Tb(III) complexes with Φ_{Tb} of 0.10 possess a limit of detection of 5 nmol (25 μM), which corresponds to 1–2 orders of magnitude greater sensitivity than clinically administered, T_1-based MRI contrast agents in phantoms and small animal imaging experiments.[51,52]

Here, we prepared samples containing complex and 10 μCi (10 μL) of ^{18}F. This amount of activity compares well to quantities used for targeted positron emission tomography (PET) imaging in small animals. Tube phantoms containing complex and ^{18}F were subsequently imaged on a small animal optical imager (top down view), with blocked excitation and open emission from 500 to 875 nm (Fig. 5A). The images acquired affirm results obtained using conventional fluorescence measurements: the "off" complex Tb(**L3**) provides no significant radiance output relative

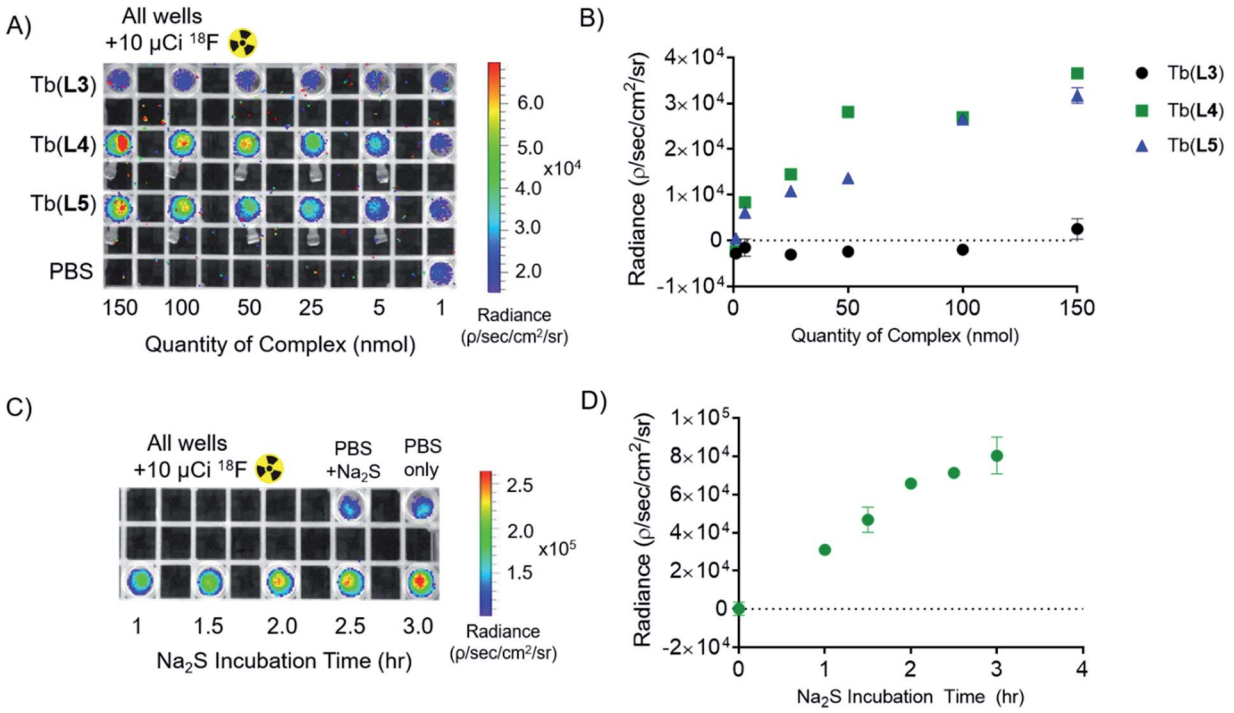

Fig. 5 Cherenkov-radiation energy transfer (CRET) imaging experiments and quantitation of detected radiance. (A) Plate image of all complexes in 200 μL of PBS buffer doped with 10 μCi $Na^{18}F$ per well. (B) Quantified radiance output of part A, buffer-only CR sample subtracted. (C) Plate image of 10 nmol Tb(**L3**) with 100 equivalents Na_2S over 3.5 hour incubation period. (D) Quantified radiance output of part C, buffer + Na_2S CR sample subtracted. Error bars represent standard deviation from ROI analysis ($n = 3$).

to ^{18}F in PBS (lower left, Fig. 5A). Region of interest (ROI) analysis of radiance indicates that turn-on complexes Tb(**L4**) and Tb(**L5**) demonstrate 220- and 190-fold radiance increase relative to Tb(**L3**) at concentrations above 25 nmol (125 μM), and a clearly discernable optical signal with only 5 nmol of complex (Fig. 5B) in accordance with our previous studies and estimates for corresponding limits of detection.

In order to observe probe turn-on in presence of a CR source, 100 equivalents of Na_2S (1000 nmol, 100 μL) were added to Tb(**L3**) (10 nmol, 100 μL). 10 μCi of ^{18}F was added to each well and samples were imaged with blocked excitation and open emission (Fig. 5C) at different lengths of Na_2S incubation (1.0, 1.5, 2.0, 2,5, 3.0, and 3.5 hours) following Na_2S addition. A 480-fold emission turn-on is observed from the *in situ* formation of Tb(**L4**) at 3.5 hours, quantified as radiance increase (Fig. 5D) relative to ^{18}F in PBS. By utilizing Cherenkov radiation, this Na_2S-reduction experiment demonstrates the first example of an analyte sensing platform with broad applicability and facile detection of lanthanide turn-on in absence of a short-wave laser excitation source or time resolution.

Conclusions

Herein, we report a new approach to generate lanthanide-based optical imaging turn-on probes through the direct chemical modification of the antenna triplet state and relative rates of back energy transfer (BET). We validated our rational design by estimating respective S_1 and T_1 states prior to synthesis and photophysical complex characterization of three pyridine-functionalized, aza-macrocycle-based Tb(III) complexes. Experimentally determined S_1 and T_1 states affirmed computationally predicted trends, but showed a 3000–8000 cm^{-1} deviation of the predicted energy levels which is consistent with previous literature findings, and therefore directly guides subsequent ligand design strategies.[53] The water-soluble Tb(III) complex series illustrates how conversion of the nitro-pyridine functionalized complex Tb(**L3**) to the corresponding amino-pyridine Tb(**L4**) or fluoro-pyridine Tb(**L5**) functionalized macrocyclic complexes results in a blue-shift of corresponding S_1 and T_1 states.

The increased energy gap between the antenna T_1 state and the $^5D_4$ Tb(III) excited state results in decreased BET efficiency for Tb(**L4**) and Tb(**L5**) complexes, which produces 500- and 465-fold increases in relative lanthanide-based quantum yield Φ_{Tb}. This is the largest increase in quantum yield reported for discrete, biocompatible lanthanide complexes (Table S1†). As a proof-of-concept, we demonstrate that turn-on of Tb(**L4**) emission by reductive, chemical transformation from Tb(**L3**) with Na_2S, an *in situ* source of hydrogen sulfide, is feasible. We employed *in situ* excitation using Cherenkov radiation to detect as little as 5 nmol of Tb(**L4**) and Tb(**L5**) with conventional, small animal optical imaging equipment. The turn-on probe design employed here obviates the need for large probe quantities otherwise incompatible with biological applications or time-resolved deconvolution typical for luminescent lanthanide-based probes to identify the desired luminescence turn-on. Furthermore, we also note that the probe concentration required to produce a detectable optical signal with Tb(**L4**) correlates closely with probe concentrations recently used to validate organic turn-on sensors *in vitro* and *in vivo*.[54,55]

While we successfully employed H_2S as a proof-of-concept turn-on analyte, we note that quantities employed here are at the upper limit of biologically encountered analyte concentration range. Future studies will focus on enhancing reactivity of Tb(III) complexes, broadening the scope of analytes that elicit a detectable turn-on response, and direct *in vivo* validation of our CR-mediated sensing approach. Second generation probes with enhanced sensitivity will be especially suitable for analyte-based, preclinical imaging in small animals or intrasurgical detection requiring limited depth penetration. We also note that Tb(**L5**) is suitable for the synthesis of a self-illuminating CR probe by incorporation of radioactive ^{18}F to displace the NO_2 functional group.

Experimental section

All starting materials were purchased from Acros Organics, Alfa Aesar, Sigma Aldrich, or TCI America and used without further purification. NMR spectra (^1H, ^{13}C, ^{19}F) were collected on a 700 MHz AdvanceIII Bruker, 500 MHz or 400 MHz Bruker instrument at 25 °C and processed using TopSpin 4.0.6. Chemical shifts are reported as parts per million (ppm). Mass spectrometry: low-resolution electrospray ionization (ESI) mass spectrometry and high-resolution ESI mass spectrometry were carried out at the Stony Brook University Institute for Chemical Biology and Drug Discovery (ICB&DD) Mass Spectrometry Facility with an Agilent LC/MSD and Agilent LC-UV-TOC spectrometers respectively. Preparative HPLC was carried out using a Shimadzu HPLC-20AR equipped with a Binary Gradient, pump, UV-Vis detector, and manual injector. Method A (preparative purification method, on Phenomenex Luna 10 μm C18 column [250 mm × 21.2 mm, 100 Å, AXIA packed]): A = 0.1% TFA in water, B = 0.1% TFA in MeCN. Gradient: 0–1 min: 5% B, 1–5 min: 5–35% B, 5–23.5 min: 35–75% B, 23.5–24 min: 75–95% B, 24–26 min: 95% B, 27–30.1 min 95–5% B. Method B preparative purification method, (preparative purification method, on Phenomenex Luna 10 μm C18 column [250 mm × 10 mm, 100 Å, AXIA packed]): $A = 10^{-2}$ M ammonium formate in water, B = 10% 10 mM ammonium formate in water, 90% MeCN. Gradient: 0–1 min: 5% B, 1–5 min: 5–35% B, 5–23.5 min: 35–75% B, 23.5–24 min: 75–95% B, 24–26 min: 95% B, 27–30.1 min 95–5% B. Analytical HPLC analysis was carried out using a Shimadzu HPLC-20AR equipped with a binary gradient, pump, UV-Vis detector, and autoinjector on a Phenomenex Luna 5 μm C18 column (150 mm × 3 mm, 100 Å, AXIA packed). Method C (analysis of Ln(III)-complexes): A = 0.1% TFA in water, B = 0.1% TFA in MeCN with a flow rate of 0.8 mL min^{-1}, UV detection at 220 and 254 nm. Gradient: 0–5 min: 95% A. 5–24 min: 5–95% B gradient. CombiFlash purifications were performed on RediSep RF Gold C18 column (50G, 100 Å) using Method D (A = 0.1% TFA in water, B = 0.1% TFA in MeCN. Gradient: 0–1.4 CV: 10% B, 1.4–2.1 CV: 10–20% B, 2.1–17.1 CV: 20–50% B, 17.1–21.9 CV: 50–100%, 21.9–23 CV: 100% B, 23–24.1 CV 10% B. Flow rate: 40 mL min^{-1}).

UV-VIS spectra were collected with a NanoDrop ^1C instrument (AZY1706045). Spectra were recorded from 200 to 900 nm in

a quartz cuvette with 1 cm path length. Room temperature luminescence measurements were carried out on a Hitachi F-7100 FL spectrophotometer at room temperature in Dulbecco's phosphate-buffered saline (DPBS). Wavelength scans were collected by exciting at the appropriate wavelength for antenna-mediated excitation and minimization of scattering interference. Luminescence emission spectra were collected under luminescence scan mode: excited at λ_{ex} (Table S6†) with emission collection from 300 to 800 nm; 1.0 nm excitation and 5.0 nm emission slit widths, chopping speed of 40 Hz, 1200 nm min^{-1} scan speed, 0.5 s response time, PMT voltage = 400 V. Lifetime measurements were executed using the following settings: Scan time 20 ms; chopping speed of 40 Hz; excitation wavelength specific to each complex (Table S6†) and emission wavelength of 545.0 nm; 0 second delay; excitation and emission slit widths of 10 nm each; 0.5 second response. Complexes were dissolved in DPBS buffer or D_2O (samples were resuspended and lyophilized in D_2O repeatedly prior to measurement). A quartz cuvette with a 1 cm pathlength was used. ICP-OES was carried out using an Agilent 5110 ICP-OES. A 10-point standard with respect to terbium was used and fits were found to be with R^2 of 0.9999. Concentrations were then back-calculated to the stock sample concentration. Concentrations of each lanthanide complex were diluted based on stock concentrations determined by ICP-OES. IVIS Lumina Series II from Caliper LifeScience small animal imager was used to image phantoms. All scans were collected with blocked excitation, open emission filter (500–875 nm, average band width 20 nm), and a collection time of 5 minutes. Images were analyzed with Living Image software version 4.3.1. Regions of interest were determined in triplicate with the ROI tool for each sample. Radiance values for each complex were subtracted from the Cherenkov-only sample ($Na^{18}F$ in PBS). Lanthanide complexation, general procedure: $Tb(OTf)_3$ (1.2 equiv.) or $GdCl_3 \cdot 6H_2O$ (1.2 equiv.) was added to a solution of ligand (1 equiv.) in 1.0 mL of water. The pH was adjusted to 7.0 with 1 M NaOH and stirred at room temperature overnight. Crude complex was loaded onto a C18 SepPak cartridge and extracted with 8 mL of 100:0 H_2O:MeCN to 70:30 H_2O:MeCN gradient. The fractions containing product were pooled and lyophilized, resulting in a white solid. Further purification under method B was applied as necessary.

Na_2S turn-on

For all *in situ* Na_2S experiments, quantity of Tb(**L3**) was pre-determined by ICP-OES. Na_2S stock solutions were prepared in PBS immediately prior to addition. Fluorimetry-based experiments were carried out by diluting 10 nmol of Tb(**L3**) in PBS and adding 100 equivalents Na_2S for a final volume of 1 mL. The reaction was monitored *via* luminescence emission from a conventional fluorimeter under the identical conditions listed above (λ_{ex} = 260 nm). For HPLC verification of Tb(**L3**) *in situ* reduction, 10 nmol of Tb(**L3**) in 100 μL was activated with 100 equivalents of Na_2S (100 μL). Selectivity experiments were conducted in the same manor, with 10 nmol of complex and 100 equivalents of Na_2S in a total volume of 1 mL PBS. I_0 was measured after 5 minutes of incubation with each respective analyte/inorganic salt (each pre-formed stock solutions in PBS); I_t was measured after 5 hours. Fold-increase of intensity is measured as I_t *vs.* I_0 of the Tb(III) peak at 548 nm. The Cherenkov-radiation imaging experiment was also carried out with 10 nmol of Tb(**L3**) in 100 μL PBS and activated with 100 equivalents of Na_2S (100 μL) for time points 1.0, 1.5, 2.0, 2.5, 3.0, and 3.5 hours prior to ^{18}F addition and imaging.

Macrocyclic starting material tri-*tert*-butyl 1,4,7,10-tetraazacyclododecane-1,4,7-triacetate (*tert*-butyl DO3A) was prepared according to literature procedure.[56] Bromo-4-fluoropyridine was also synthesized in one step from commercially available 2-methyl-4-fluoropyridine in one step according to a patented procedure.[57]

{4,10-Bis(carboxymethyl)-7-[(4-nitro-2-pyridyl)methyl]-1,4,7,10-tetraaza-1-cyclododecyl}acetic acid, L3

Tert-Butyl {4,10-bis(*tert*-butoxycarbonylmethyl)-7-[(4-nitro-2-pyridyl)methyl]-1,4,7,10-tetraaza-1-cyclododecyl}acetate, **S1**, (34.1 mg, 0.023 mmol) was added to a 2:1 solution of TFA and DCM and stirred overnight at room temperature. The solvent was removed *in vacuo*, and the product was re-dissolved in H_2O. The solution was then lyophilized to yield **L3** as an off-white solid (11.1 mg, 0.022 mmol, R_t (method C) = 3.0 minutes). ^1H NMR (CD_3OD, 500 MHz): δ 8.88 (d, 1H), 8.23 (s, 1H), 8.10 (s, 1H), 4.13 (br s, 2H), 3.76–3.57 (m, 16H), 3.23–3.21 (m, 6H). ^{13}C NMR (CD_3OD, 125 MHz): δ 173.12, 169.36, 159.54, 156.12, 152.71, 117.43, 116.77, 58.33, 55.34, 54.12, 52.25, 50.48, 49.62. ESI-MS calcd. for $C_{20}H_{30}N_6O_8$: 482.2125. Found: 483.2198 $[M + H]^+$.

{10-[(4-Amino-2-pyridyl)methyl]-4,7-bis(carboxymethyl)-1,4,7,10-tetraaza-1-cyclododecyl}acetic acid, L4

Tert-Butyl {10-[(4-amino-2-pyridyl)methyl]-4,7-bis(*tert*-butoxycarbonylmethyl)-1,4,7,10-tetraaza-1-cyclododecyl}acetate, **S2**, (7.1 mg, 0.011 mmol) was added to a 2:1 solution of TFA and DCM and stirred overnight at room temperature. The solvent was removed *in vacuo*, and the product was re-dissolved in H_2O. The solution was then lyophilized to yield **L4** as an off-white solid (4.7 mg, 0.010 mmol, (method C) = 1.89 minutes). ^1H NMR (CD_3OD, 400 MHz): 7.90 (d, 1H), 6.86 (s, 1H), 6.72 (d, 2H), 4.07 (br s, 2H), 3.96–3.66 (m, 4H), 3.26–2.93 (m, 18H). ^{13}C NMR (CD_3OD, 100 MHz): δ 177.27, 176.46, 175.85, 161.89, 149.85, 142.07, 111.23, 109.06, 57.47, 56.14, 56.13, 55.44, 54.34, 51.78. ESI-MS calcd. for $C_{20}H_{32}N_6O_6$: 452.2383. Found: 453.2457 $[M + H]^+$.

{4,10-Bis(carboxymethyl)-7-[(4-fluoro-2-pyridyl)methyl]-1,4,7,10-tetraaza-1-cyclododecyl}acetic acid, L5

Tert-Butyl {4,10-bis(*tert*-butoxycarbonylmethyl)-7-[(4-fluoro-2-pyridyl)methyl]-1,4,7,10-tetraaza-1-cyclododecyl}acetate, **S3**, (15.2 mg, 0.023 mmol) was added to a 2:1 solution of TFA and DCM and stirred overnight at room temperature. The solvent was removed *in vacuo*, and the product was re-dissolved in H_2O. The solution was then lyophilized to yield **L5** as an off-white solid (97%, 10.3 mg, 0.023 mmol, (method C) = 2.01 minutes). ^1H NMR (CD_3OD, 400 MHz): δ 8.58 (m, 1H), 7.35 (d, 1H), 7.22 (m, 1H), 4.62 (br s, 2H), 4.11 (br s, 2H), 3.69–3.49 (m, 14H), 3.22 (m, 6H). ^{13}C NMR (CD_3OD, 125 MHz): δ 173.05,

172.01, 169.91, 158.79, 153.12, 120.96, 118.64, 116.34, 58.17, 55.77, 53.82, 52.61, 51.37, 50.75, 50.17. ^{19}F NMR: (CD_3OD, 376 MHz): −100.16. (CD_3OD, 376 MHz): ESI-MS calcd. for $C_{20}H_{30}FN_5O_6$: 455.2180. Found: 456.2256 $[M + H]^+$.

Tb(L3). Calculated monoisotopic mass for ($C_{20}H_{27}N_6O_8Tb$): 638.1144; found: m/z = 639.1217 $[M + H]^+$. R_t = 2.13 min (Method C).

Tb(L4). Calculated monoisotopic mass for ($C_{20}H_{29}N_6O_6Tb$): 608.1402; found: m/z = 609.1475 $[M + H]^+$. R_t = 1.82 min (Method C).

Tb(L5). Calculated monoisotopic mass for ($C_{20}H_{27}FN_5O_6Tb$): 611.1199; found: m/z = 634.1093$[M + Na]^+$. R_t = 2.03 min (Method C).

Gd(L3). Calculated monoisotopic mass for ($C_{20}H_{27}N_6O_8Gd$): 637.1131; found: m/z = 660.1025 $[M + Na]^+$. R_t = 2.13 min (Method C).

Gd(L4). Calculated monoisotopic mass for ($C_{20}H_{29}N_6O_6Gd$): 607.1390; found: m/z = 608.1468 $[M + H]^+$. R_t = 1.58 min (Method C).

Gd(L5). Calculated monoisotopic mass for ($C_{20}H_{27}FN_5O_6$-Gd): 610.1186; found: m/z = 633.1097 $[M + Na]^+$. R_t = 1.97 min (Method C).

Computational details

DFT calculations were performed using the Gaussian 16 software.[58] The starting geometries for the complexes were taken from the crystal structure of a similar complex.[59] Geometries of the complexes were optimized in the gas phase at 298 K using the TPSSh functional.[60] Light atoms (H, N, C, O, F) were treated with the 6-31G(d,p) basis set, and the Tb(III) center was assigned the large core relativistic effective core potential (LCRECP) and related (7s6p5d)/5s4p3d basis set.[61]) The LCRECP includes 52 electrons in the core of the metal center leaving the outermost 5s, 5p, 5d, and 6s electrons to be handled explicitly. As such, the GS calculations were performed in the pseudosinglet state and T_1 calculations were performed in the pseudotriplet state. Frequency calculations were performed at the same level of theory to confirm that the optimized structures were local minima on the potential energy surface and to determine the thermodynamic properties of the complexes. Solvation energies were calculated using the SMD method[62] and the thermodynamic properties in H_2O were estimated by taking the thermodynamic corrections from gas-phase calculations. Optimized coordinates for the complexes in the GS and T_1 states are given in the ESI.†

Data availability

Raw data for imaging and spectroscopy is available as an x, y number document upon request.

Author contributions

The manuscript was written through contributions of all authors. All authors have given approval to the final version of the manuscript.

Conflicts of interest

There are no conflicts to declare.

Acknowledgements

Financial support for this work was provided by the National Science Foundation (CHE 1942434, NSF CAREER, E. B.), the Novo Nordisk Foundation (TJS), Carlsbergfondet (TJS), Villum Fonden (grant #14922, TJS).

Notes and references

1 H. Ito, T. Terai, K. Hanaoka, T. Ueno, T. Komatsu, T. Nagano and Y. Urano, *Chem. Commun.*, 2015, **51**, 8319–8322.
2 S. C. Zondlo, F. Gao and N. J. Zondlo, *J. Am. Chem. Soc.*, 2010, **132**, 5619–5621.
3 E. Pershagen and K. E. Borbas, *Angew. Chem., Int. Ed.*, 2015, **54**, 1787–1790.
4 E. Pershagen, J. Nordholm and K. E. Borbas, *J. Am. Chem. Soc.*, 2012, **134**, 9832–9835.
5 B. K. McMahon, R. Pal and D. Parker, *Chem. Commun.*, 2013, **49**, 5363–5365.
6 J. E. Whitaker, R. P. Haugland and F. G. Prendergast, *Anal. Biochem.*, 1991, **194**, 330–344.
7 D. Parker, P. Kanthi Senanayake and J. A. Gareth Williams, *J. Chem. Soc., Perkin Trans. 2*, 1998, **2**, 2129–2140.
8 E. Del Giorgio and T. J. Sørensen, *Molecules*, 2020, **25**, 1959.
9 M. L. Aulsebrook, B. Graham, M. R. Grace and K. L. Tuck, *Tetrahedron*, 2014, **70**, 4367–4372.
10 W. Xu, Y. Zhou, D. Huang, M. Su, K. Wang and M. Hong, *Inorg. Chem.*, 2014, **53**, 6497–6499.
11 T. J. Rink, R. Y. Tsien and T. Pozzan, *J. Cell Biol.*, 1982, **95**, 189–196.
12 A. Minta, J. P. Y. Kao and R. Y. Tsien, *J. Biol. Chem.*, 1989, **264**, 8171–8178.
13 S. H. Hewitt, G. Macey, R. Mailhot, M. R. J. Elsegood, F. Duarte, A. M. Kenwright and S. J. Butler, *Chem. Sci.*, 2020, **11**, 3619–3628.
14 G. Vereb, E. Jares-Erijman, P. R. Selvin and T. M. Jovin, *Biophys. J.*, 1998, **74**, 2210–2222.
15 A. G. Cosby, S. H. Ahn and E. Boros, *Angew. Chem., Int. Ed.*, 2018, **57**, 15496–15499.
16 A. G. Cosby, G. Quevedo and E. Boros, *Inorg. Chem.*, 2019, **58**, 10611–10615.
17 M. C. Heffern, L. M. Matosziuk and T. J. Meade, *Chem. Rev.*, 2014, **114**, 4496–4539.
18 L. G. Nielsen, A. K. R. Junker and T. J. Sørensen, *Dalton Trans.*, 2018, **47**, 10360–10376.
19 S. I. Weissman, *J. Chem. Phys.*, 1942, **10**, 214–217.
20 B. Alpha, R. Ballardini, V. Balzani, J.-M. Lehn, S. Perathoner and N. Sabbatini, *Photochem. Photobiol.*, 1990, **52**, 299–306.
21 S. J. Butler, *Chem. Commun.*, 2015, **51**, 10879–10882.
22 S. Y. Huang and V. C. Pierre, *Chem. Commun.*, 2018, **54**, 9210–9213.
23 D. G. Smith, R. Pal and D. Parker, *Chem.–Eur. J.*, 2012, **18**, 11604–11613.

24 S. H. Jung, K. Y. Kim, J. H. Lee, C. J. Moon, N. S. Han, S.-J. Park, D. Kang, J. K. Song, S. S. Lee, M. Y. Choi, J. Jaworski and J. H. Jung, *ACS Appl. Mater. Interfaces*, 2017, **9**, 722–729.
25 E. Pershagen and K. E. Borbas, *Angew. Chem., Int. Ed.*, 2015, **54**, 1787–1790.
26 T. Terai, K. Kikuchi, Y. Urano, H. Kojima and T. Nagano, *Chem. Commun.*, 2012, **48**, 2234–2236.
27 M. Latva, H. Takalo, V.-M. Mukkala, C. Matachescu, J. C. Rodríguez-Ubis and J. Kankare, *J. Lumin.*, 1997, **75**, 149–169.
28 A. D'Aléo, E. G. Moore, J. Xu, L. J. Daumann and K. N. Raymond, *Inorg. Chem.*, 2015, **54**, 6807–6820.
29 A. P. S. Samuel, J. Xu and K. N. Raymond, *Inorg. Chem.*, 2009, **48**, 687–698.
30 S. Shuvaev, M. Starck and D. Parker, *Chem.–Eur. J.*, 2017, **23**, 9974–9989.
31 T. J. Sørensen and S. Faulkner, *Acc. Chem. Res.*, 2018, **51**, 2493–2501.
32 M. Woods, G. E. Kiefer, S. Bott, A. Castillo-Muzquiz, C. Eshelbrenner, L. Michaudet, K. McMillan, S. D. K. Mudigunda, D. Ogrin, G. Tircsó, S. Zhang, P. Zhao and A. D. Sherry, *J. Am. Chem. Soc.*, 2004, **126**, 9248–9256.
33 O. A. Blackburn, M. Tropiano, L. S. Natrajan, A. M. Kenwright and S. Faulkner, *Chem. Commun.*, 2016, **52**, 6111–6114.
34 E. Llobet, J. Brunet, A. Pauly, A. Ndiaye and C. Varenne, *Sensors*, 2017, **17**, 391.
35 J. Katla and S. Kanvah, *Photochem. Photobiol. Sci.*, 2018, **17**, 42–50.
36 X. Huang, H. Liu, J. Zhang, B. Xiao, F. Wu, Y. Zhang, Y. Tan and Y. Jiang, *New J. Chem.*, 2019, **43**, 6848–6855.
37 Y. L. Pak, J. Li, K. C. Ko, G. Kim, J. Y. Lee and J. Yoon, *Anal. Chem.*, 2016, **88**, 5476–5481.
38 Y. Takano, H. Echizen and K. Hanaoka, *Antioxid. Redox Signaling*, 2017, **27**, 669–683.
39 L. Babetto, S. Carlotto, A. Carlotto, M. Rancan, G. Bottaro, L. Armelao and M. Casarin, *Dalton Trans.*, 2020, **49**, 14556–14563.
40 C. Greco, G. Moro, L. Bertini, M. Biczysko, V. Barone and U. Cosentino, *J. Chem. Theory Comput.*, 2014, **10**, 767–777.
41 S.-y. Baek, S.-Y. Kwak, S.-T. Kim, K. Y. Hwang, H. Koo, W.-J. Son, B. Choi, S. Kim, H. Choi and M.-H. Baik, *Nat. Commun.*, 2020, **11**, 2292.
42 U. Cosentino, A. Villa, D. Pitea, G. Moro and V. Barone, *J. Phys. Chem. B*, 2000, **104**, 8001–8007.
43 A. Beeby, I. M. Clarkson, R. S. Dickins, S. Faulkner, D. Parker, L. Royle, A. S. d. Sousa, J. A. G. Williams and M. Woods, *J. Chem. Soc., Perkin Trans. 2*, 1999, **2**, 493–503.
44 A. K. R. Junker and T. J. Sørensen, *Dalton Trans.*, 2019, **48**, 964–970.
45 O. Kabil and R. Banerjee, *J. Biol. Chem.*, 2010, **285**, 21903–21907.
46 M. M. Gadalla and S. H. Snyder, *J. Neurochem.*, 2010, **113**, 14–26.
47 X. Wang, L. An, Q. Tian and K. Cui, *RSC Adv.*, 2019, **9**, 33578–33588.
48 Z. Dai, L. Tian, B. Song, Z. Ye, X. Liu and J. Yuan, *Anal. Chem.*, 2014, **86**, 11883–118839.
49 Y. Yao, L. Delgado-Rivera, H. Samareh Afsari, L. Yin, G. R. J. Thatcher, T. W. Moore and L. W. Miller, *Inorg. Chem.*, 2018, **57**, 681–688.
50 M. Tropiano and S. Faulkner, *Chem. Commun.*, 2014, **50**, 4696–4698.
51 J. Wahsner, E. M. Gale, A. Rodríguez-Rodríguez and P. Caravan, *Chem. Rev.*, 2019, **119**, 957–1057.
52 B. Driehuys, J. Nouls, A. Badea, E. Bucholz, K. Ghaghada, A. Petiet and L. W. Hedlund, *ILAR J.*, 2008, **49**, 35–53.
53 D. Jacquemin, B. Mennucci and C. Adamo, *Phys. Chem. Chem. Phys.*, 2011, **13**, 16987–16998.
54 Z. Chen, X. Mu, Z. Han, S. Yang, C. Zhang, Z. Guo, Y. Bai and W. He, *J. Am. Chem. Soc.*, 2019, **141**, 17973–17977.
55 M. Y. Lucero, A. K. East, C. J. Reinhardt, A. C. Sedgwick, S. Su, M. C. Lee and J. Chan, *J. Am. Chem. Soc.*, 2021, **143**, 7196–7202.
56 K. Kikuchi, F. Sugihara, S. Mizukami, Y. Yoshioka, H. Matsushita and T. Nakamura, *Angew. Chem., Int. Ed.*, 2014, **54**, 1007–1010.
57 R. Blunt, A. J. Eatherton, V. Garzya, M. P. Healy, J. Myatt and R. A. Porter, WO2011012622A1, 2011.
58 M. J. Frisch, G. W. Trucks, H. B. Schlegel, G. E. Scuseria, M. A. Robb, J. R. Cheeseman, G. Scalmani, V. Barone, G. A. Petersson, H. Nakatsuji, X. Li, M. Caricato, A. V. Marenich, J. Bloino, B. G. Janesko, R. Gomperts, B. Mennucci, H. P. Hratchian, J. V. Ortiz, A. F. Izmaylov, J. L. Sonnenberg, D. Williams-Young, F. Ding, F. Lipparini, F. Egidi, J. Goings, B. Peng, A. Petrone, T. Henderson, D. Ranasinghe, V. G. Zakrzewski, J. Gao, N. Rega, G. Zheng, W. Liang, M. Hada, M. Ehara, K. Toyota, R. Fukuda, J. Hasegawa, M. Ishida, T. Nakajima, Y. Honda, O. Kitao, H. Nakai, T. Vreven, K. Throssell, J. A. Montgomery Jr, J. E. Peralta, F. Ogliaro, M. J. Bearpark, J. J. Heyd, E. N. Brothers, K. N. Kudin, V. N. Staroverov, T. A. Keith, R. Kobayashi, J. Normand, K. Raghavachari, A. P. Rendell, J. C. Burant, S. S. Iyengar, J. Tomasi, M. Cossi, J. M. Millam, M. Klene, C. Adamo, R. Cammi, J. W. Ochterski, R. L. Martin, K. Morokuma, O. Farkas, J. B. Foresman and D. J. Fox, *Gaussian 16 Rev. C01*, Wallingford, CT, 2016.
59 S. Aime, A. S. Batsanov, M. Botta, J. A. K. Howard, M. P. Lowe and D. Parker, *New J. Chem.*, 1999, **23**, 669–670.
60 J. Tao, J. P. Perdew, V. N. Staroverov and G. E. Scuseria, *Phys. Rev. Lett.*, 2003, **91**, 146401.
61 A. Nicklass, M. Dolg, H. Stoll and H. Preuss, *J. Chem. Phys.*, 1995, **102**, 8942–8952.
62 A. V. Marenich, C. J. Cramer and D. G. Truhlar, *J. Phys. Chem. B*, 2009, **113**, 6378–6396.